Published in final edited form as:

Biochemistry. 2021 August 24; 60(33): 2519–2523. doi:10.1021/acs.biochem.1c00342.

Quantitative NMR study of insulin degrading enzyme using amyloid-β and HIV-1 p6 elucidates its chaperone activity

Bhargavi Ramaraju[†], **Spencer L. Nelson**[†], **Wenwei Zheng**[‡], **Rodolfo Ghirlando**[§], **Lalit Deshmukh**[†]

[†]Department of Chemistry and Biochemistry, University of California San Diego, La Jolla, California 92093, United States.

[‡]College of Integrative Sciences and Arts, Arizona State University, Mesa, Arizona 85212, United States.

[§]Laboratory of Molecular Biology, National Institute of Diabetes and Digestive and Kidney Diseases, National Institutes of Health, Bethesda, Maryland 20892, United States.

Abstract

Insulin degrading enzyme (IDE) hydrolyzes monomeric polypeptides, including amyloid-β (Aβ) and HIV-1 p6. It also acts as a non-proteolytic chaperone to prevent Aβ polymerization. Here we compare interactions of Aβ and nonamyloidogenic p6 with IDE. Although both exhibited similar proteolysis rates, the binding kinetics to an inactive IDE characterized using relaxation-based NMR were remarkably different. IDE and Aβ formed a sparsely populated complex with a lifetime of milliseconds in which a short hydrophobic cleavage segment of Aβ was anchored to IDE. Strikingly, a second and more stable complex was significantly populated with a sub-second lifetime owing to multiple intermolecular contacts between Aβ and IDE. By selectively sequestering Aβ in this non-productive complex, IDE likely increases the critical concentration required for fibrilization. In contrast, IDE and p6 formed a transient, sub-millisecond complex involving a single anchoring p6 motif. Modulation of intermolecular interactions, thus, allows IDE to differentiate between non- and amyloidogenic substrates.

Graphical Abstract

Corresponding Author, ldeshmukh@ucsd.edu.

Supporting Information

The Supporting Information is available free of charge on the ACS Publications website.

Experimental details, fitting procedures, 12 additional figures, and 4 tables (PDF)

Accession Codes

HIV-1 p6 (Uniprot accession no. P04591), Human IDE (Uniprot accession no. P14735), Aβ42/40 (Uniprot accession no. E9PG40). HIV-1 p6 construct has been deposited in the Addgene repository, https://www.addgene.org; accession no. 154201. The chemical-shift assignments of p6 have been deposited in the Biological Magnetic Resonance Bank, http://www.bmrb.wisc.edu; accession no. 50916.

The authors declare no competing financial interests.

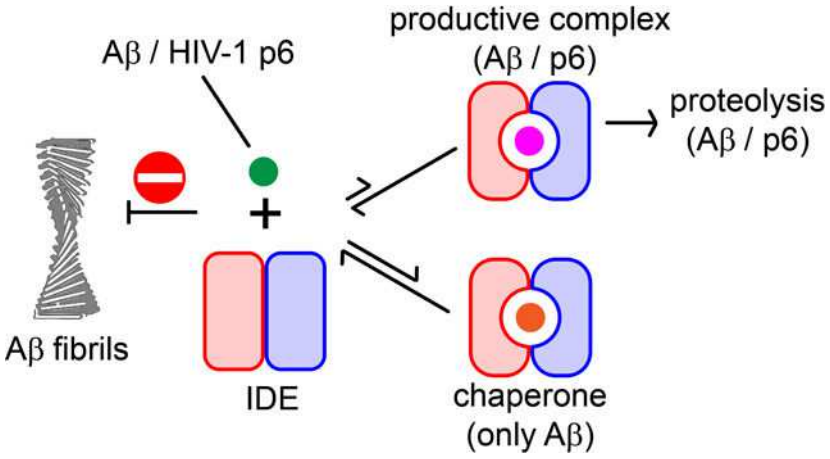

Human insulin degrading enzyme (IDE) is a dimeric metalloprotease involved in proteostasis, a regulatory mechanism responsible for preventing misfolded protein aggregates.[1–3] It hydrolyzes diverse polypeptides, including insulin, amyloid-β (Aβ), and HIV-1 p6.[4] Remarkably, it also functions as a chaperone by forming a proteolysis-independent kinetic trap for amyloidogenic substrates such as Aβ.[5–7] This activity likely involves confinement of substrate by IDE, followed by its controlled disposal, similar to that of heat-shock proteins (HSPs) and IDE was shown to exhibit HSP-like expression.[8]

To study the chaperone activity of IDE, we compared Aβ42 and Aβ40 to nonamyloidogenic, soluble p6 (Figure 1A). Inactive IDE for binding analyses was prepared by a point mutation (IDE_{E111Q}).[9] Aβ42 and Aβ40 are the two major Aβ isoforms;[10] Aβ42 is more aggregation prone than Aβ40.[11] The conditions used for NMR, namely dilute samples (≤50 μM) maintained at 2 °C, did not support Aβ fibrilization.[12] ^{15}N-labeled Aβ42, Aβ40, and p6 were incubated with IDE and NMR spectra were recorded as proteolysis progressed (Figures S1–S2). Significant reduction in $^{1}H_N/^{15}N$ cross-peak heights was observed for residues 10–27 of Aβ42 and residues 484–495 of p6 (Figure 1B–C), indicating that these segments represent the cleavage sites.

Residues 10–13 and 14–19 (without outlier Q15) of Aβ42 could be grouped in clusters exhibiting slow and fast decay kinetics, respectively (Figure 1D). These results agree with a prior mass spectrometry (MS) study[14] of Aβ42 – IDE interactions that identified cleavage sites between residues 13–14 and 19–20. The site-specific decay of cumulative cross-peak heights was fit to a rate equation, yielding rates of 48±3 and 101±5 pmol/min for cleavages at positions 13–14 and 19–20, respectively (Figure 1D). The MS study[14] also identified cleavage at position 14–15, and secondary hydrolysis at sites 18–19, 20–21, 28–29 of Aβ42. Q15 exhibited a different attenuation profile relative to residues 14–19 (Figure 1B). Proteolysis at secondary sites could not be deciphered unambiguously. IDE-mediated degradation of Aβ40 produced comparable results (Figure S2), establishing that Aβ42 and Aβ40 are similarly hydrolyzed.

Residues 484–495 (excluding outlier G494) of p6 exhibited similar attenuation profiles upon IDE-mediated degradation (Figure 1E). An MS study[4] of p6 – IDE interactions

identified cleavage at 463–464, 473–474, and 489–490. Thus, we determined the cleavage site to be at 489–490. The lack of proteolysis at the other two sites can be attributed to different constructs used in these two studies (Figure S3). The MS study[4] also identified 7 auxiliary cleavage sites (clustered around motifs 460–464, and 485–493). Based on the lack of attenuation for 460–464 and the uniform decay of 485–493, we conclude that these cleavages were not observed, likely due to digestion temperature differences, 2 °C (NMR) vs. 37 °C (MS). An apparent rate constant of 30±1 pmol/min was obtained for 489–490 cleavage (Figure 1E).

The catalytically inactive IDE_{E111Q}, with and without substrates, was dimeric by analytical ultracentrifugation (Figure S4). It is not amenable to traditional NMR due to fast transverse relaxation rates (R_2), stemming from its large size (~230 kDa; ^{15}N-R_2 rates of IDE_{E111Q} dimer were estimated to be ~400 s^{-1} at 2 °C and 800 MHz[15]). IDE_{E111Q}-bound states of Aβ/p6 can, therefore, be categorized as NMR-invisible states. To investigate the binding kinetics of Aβ/p6 to IDE_{E111Q}, we used relaxation-based NMR methods.[16] Figure 2A displays a correlation plot of the differences observed in ^{15}N-R_2 values of Aβ42 recorded with and without IDE_{E111Q} at 600 and 800 MHz (lifetime line-broadening; ^{15}N-ΔR_2)[12]. ^{15}N-ΔR_2 values were field-independent, a characteristic of slow-exchange between free and IDE_{E111Q}-bound Aβ42 on the transverse relaxation timescale.[16] These observations were consistent with the lack of ^{15}N-exchange-induced chemical shifts[17] (^{15}N-δ^{ex}; Figure S5) and ^{15}N-Carr-Purcell-Meiboom-Gill (CPMG) relaxation dispersions[18] (SI) for Aβ42 + IDE_{E111Q} sample. Significant broadening of ^{15}N dark-state exchange saturation transfer (DEST)[12] profiles was observed for all Aβ42 residues with IDE_{E111Q} (Figures 2B, S6). Relatively uniform ^{15}N-ΔR_2 values (2.5–5 s^{-1}) were observed for Aβ42 residues, with residues 18–20 exhibiting slightly elevated values of 4–5 s^{-1} (Figure 2C). Because the latter comprise the cleavage site (cf. Figure 1B), the ^{15}N-DEST/ΔR_2 effects described above likely originate from the binding of Aβ42 to the active site of IDE_{E111Q}.

Not all ^{15}N-DEST/ΔR_2 profiles could fit a two-state model comprising free and bound Aβ42, indicating the presence of multiple bound states (sedimentation analysis established that unbound Aβ42 remains predominantly monomeric, Figure S7). The kinetic model that accounted for all NMR data (Figure 2D) comprised a three-state exchanging system where NMR-visible Aβ42 (State **A**) exchanges with two NMR-invisible IDE-bound species (States **B** and **C**). It was selected based on prior evidence,[6] demonstrating that Aβ42 – IDE interactions result in hydrolysis or the formation of a proteolysis-independent complex. The yield of the latter was increased ~3–10-fold upon IDE inhibition.[7] Thus, we argue that among the two IDE-bound states, one is primed for proteolysis, and the other is a kinetic trap.

Simultaneous fitting of ^{15}N-DEST/ΔR_2 profiles to the three-state model via propagation of the Bloch-McConnell equations[19] yielded rate constants, populations, and transverse relaxation rate profiles (^{15}N-R_2^{Bound}) of the two IDE-bound states (Figures 2D–E, Table S1). Under the experimental conditions (Aβ42 + IDE_{E111Q}, 50 μM each), State **B** was sparsely populated (~2%) with a lifetime of ~5 ms, association (k_{on}) and dissociation (k_{off}) rate constants of ~11 × 10^4 $M^{-1}s^{-1}$ and ~180 s^{-1}, respectively, and an equilibrium dissociation

constant, K_D, of ~1.6 mM (Table S2). For State **B**, residues 18–20 were most immobilized upon binding with the average $<^{15}N\text{-}R_2^{Bound}>$ value of ~370 s^{-1} (Figure 2E). Stabilization of the IDE catalytic site by residues 18–19 of Aβ42 via a β-strand conformation is vital for hydrolysis.[20] Thus, we conclude that State **B** represents an Aβ42 conformation comprising a short β-strand, which an active enzyme can hydrolyze. State **C** was populated at ~16%, with lifetime ~0.1 s, k_{on} ~3×10^4 $M^{-1}s^{-1}$, k_{off} ~7 s^{-1}, and K_D ~0.2 mM (Table S2). The average $<^{15}N\text{-}R_2^{Bound}>$ values of residues 3–5 and 8–12 were ~350 and 370 s^{-1} at 800 MHz, respectively, implying that these segments were immobilized upon binding (Figure 2E). The average $<^{15}N\text{-}R_2^{Bound}>$ values for regions 16–26 and 28–42 were ~250 s^{-1}, indicating that these segments interact with IDE_{E111Q} to form multiple bound conformations that interconvert on a timescale shorter than the lifetime of the complex. The presence of multiple binding motifs results in ~20-fold increase in the lifetime of State **C** relative to that of State **B**. Thus, we conclude that State **C** represents a kinetic trap. Simultaneous fitting of ^{15}N-DEST/ΔR_2 profiles of Aβ40 recorded with IDE_{E111Q} generated comparable results (Figure S8, Tables S1–2). These Aβ – IDE_{E111Q} interactions, particularly the presence of multiple anchoring motifs, are similar to that of the interactions between Aβ and bacterial chaperonin, GroEL.[15, 21] Note that the latter, however, are highly transient (lifetime ≤ ms). The nonproteolytic Aβ – IDE_{E111Q} interactions prevented Aβ fibrilization at 37 °C (Figure 3; also see Figure S9), implying that they compete with Aβ self-association. Hence, IDE_{E111Q} likely increases the critical concentration required for Aβ fibrilization.

The ^{15}N-ΔR_2 profiles of p6 recorded with IDE_{E111Q} were field-dependent (Figure 4A), a hallmark of the fast-exchange regime.[16] The latter is manifested by the presence of small ^{15}N-δ^{ex} values, which did not correlate with ^{15}N-ΔR_2 values (Figure S10A). The average ^{15}N-ΔR_2 values of p6 were linearly dependent on IDE_{E111Q} (Figure S10B–C). Hence, the increase in ^{15}N-ΔR_2 values of p6 on the addition of IDE_{E111Q} stems from their association. Examples of ^{15}N-DEST and CPMG profiles and plots of ^{15}N-δ^{ex} values and ^{15}N-ΔR_2 rates for p6 with IDE_{E111Q} are shown in Figures 4B–E; also see Figure S11. Only F493 exhibited a noticeable CPMG dispersion (R_{ex} ~2 s^{-1}), consistent with the observation that F493 also exhibited the largest ^{15}N-δ^{ex} value with IDE_{E111Q} (−5 Hz; inclusion of CPMG dispersions in DEST/ΔR_2 analyses allowed us to decorrelate the population of bound p6 from R_2^{Bound} for the fast-exchange regime[16]).

Unlike Aβ, excellent global fits were obtained using a two-state exchange model, comprising free (State **A**) and bound p6 (State **B**), Figure 4F, S10. Under the experimental conditions (p6 + IDE_{E111Q}, 500 μM each), State **B** was populated at ~3%, with lifetime ~140 μs, k_{on} ~50×10^4 $M^{-1}s^{-1}$, k_{off} ~7000 s^{-1} and K_D ~14 mM (Table S3), establishing the weak nature of this interaction at 2 °C. Residues 480–496 exhibited large ^{15}N-R_2^{Bound} values (≥100 s^{-1}, Figure 4G, Table S4), with F493 exhibiting the largest value of ~390 s^{-1} (800 MHz). The largest calculated differences in ^{15}N shifts (^{15}N-Δδ) between free and IDE-bound p6 was also observed for F493 (−2.1 ppm at 800 MHz; Figure S12). ^{15}N-Δδ values were ≤ ppm for all other residues, implying an ensemble of random coil conformations in the IDE-bound state. These observations imply that State **B** likely represents a productive complex and that the absence of β-strand conformation and of multiple anchoring motifs

result in a rapid release of IDE-bound p6. IDE, thus, employs a different binding mode for nonamyloidogenic p6.

Thus, Aβ and IDE form either a sparsely populated complex that can be proteolyzed or a major complex that selectively entraps Aβ. Multiple intermolecular contacts increase the lifetime of the latter. Because a substoichiometric amount of inactive IDE prevents Aβ fibrilization, these nonproteolytic interactions are likely responsible for IDE's chaperone activity. The latter is likely due to a reduction in the population of Aβ oligomers that self-associate to form fibrils. Whether IDE can bind and disaggregate Aβ aggregation nuclei required for fibril formation is unclear, and studies to understand the underlying mechanism are currently ongoing in our laboratory. Only a single productive complex is formed with p6. It is short-lived owing to a significant reduction in the intermolecular interactions, thereby allowing IDE to differentiate between non- and amyloidogenic substrates.

Supplementary Material

Refer to Web version on PubMed Central for supplementary material.

ACKNOWLEDGMENT

We thank Z. Jiang, V. Tugarinov, M. Wälti, A. Ceccon, and P. A. Jennings for useful discussions, X. Huang, and J. Yu for NMR support. This work was funded, in part, by a 2018 Development Award from the San Diego Center for AIDS Research (NIH Grant P30 AI036214) (to L.D.); by Collaborative Development Award from the HIV Interactions in Viral Evolution Center (The Scripps Research Institute; NIH Grant U54 AI150472) (to L.D.). R.G. was supported by the Intramural Research Program at the NIH. W.Z. acknowledges the support from the NSF (MCB-2015030) and the research computing at Arizona State University.

REFERENCES

1. Tang W-J, Targeting insulin-degrading enzyme to treat type 2 diabetes mellitus. Trends Endocrinol. Metab 2016, 27 (1), 24–34. [PubMed: 26651592]
2. Kurochkin IV; Guarnera E; Berezovsky IN, Insulin-degrading enzyme in the fight against Alzheimer's disease. Trends Pharmacol. Sci 2018, 39 (1), 49–58. [PubMed: 29132916]
3. Tundo GR; Sbardella D; Ciaccio C; Grasso G; Gioia M; Coletta A; Polticelli F; Di Pierro D; Milardi D; Van Endert P; Marini S; Coletta M, Multiple functions of insulin-degrading enzyme: a metabolic crosslight? Crit. Rev. Biochem. Mol. Biol 2017, 52 (5), 554–582. [PubMed: 28635330]
4. Hahn F; Schmalen A; Setz C; Friedrich M; Schlosser S; Kolle J; Spranger R; Rauch P; Fraedrich K; Reif T; Karius-Fischer J; Balasubramanyam A; Henklein P; Fossen T; Schubert U, Proteolysis of mature HIV-1 p6 Gag protein by the insulin-degrading enzyme (IDE) regulates virus replication in an Env-dependent manner. PLoS One 2017, 12 (4), e0174254. [PubMed: 28388673]
5. Llovera RE; de Tullio M; Alonso LG; Leissring MA; Kaufman SB; Roher AE; de Prat Gay G; Morelli L; Castaño EM, The catalytic domain of insulin-degrading enzyme forms a denaturant-resistant complex with amyloid beta peptide: implications for Alzheimer disease pathogenesis. J. Biol. Chem 2008, 283 (25), 17039–48. [PubMed: 18411275]
6. de Tullio MB; Morelli L; Castaño EM, The irreversible binding of amyloid peptide substrates to insulin-degrading enzyme: a biological perspective. Prion 2008, 2 (2), 51–56. [PubMed: 19098445]
7. de Tullio MB; Castelletto V; Hamley IW; Martino Adami PV; Morelli L; Castaño EM, Proteolytically inactive insulin-degrading enzyme inhibits amyloid formation yielding non-neurotoxic Aβ peptide aggregates. PLoS One 2013, 8 (4), e59113. [PubMed: 23593132]
8. Tundo GR; Sbardella D; Ciaccio C; Bianculli A; Orlandi A; Desimio MG; Arcuri G; Coletta M; Marini S, Insulin-degrading enzyme (IDE): a novel heat shock-like protein. J. Biol. Chem 2013, 288 (4), 2281–2289. [PubMed: 23188819]

9. Perlman RK; Gehm BD; Kuo WL; Rosner MR, Functional analysis of conserved residues in the active site of insulin-degrading enzyme. J. Biol. Chem 1993, 268 (29), 21538–21544. [PubMed: 8104941]

10. Wilquet V; De Strooper B, Amyloid-beta precursor protein processing in neurodegeneration. Curr. Opin. Neurobiol 2004, 14 (5), 582–8. [PubMed: 15464891]

11. Bateman RJ; Xiong C; Benzinger TL; Fagan AM; Goate A; Fox NC; Marcus DS; Cairns NJ; Xie X; Blazey TM; Holtzman DM; Santacruz A; Buckles V; Oliver A; Moulder K; Aisen PS; Ghetti B; Klunk WE; McDade E; Martins RN; Masters CL; Mayeux R; Ringman JM; Rossor MN; Schofield PR; Sperling RA; Salloway S; Morris JC, Clinical and biomarker changes in dominantly inherited Alzheimer's disease. N. Engl. J. Med 2012, 367 (9), 795–804. [PubMed: 22784036]

12. Fawzi NL; Ying J; Ghirlando R; Torchia DA; Clore GM, Atomic-resolution dynamics on the surface of amyloid-beta protofibrils probed by solution NMR. Nature 2011, 480 (7376), 268–72. [PubMed: 22037310]

13. Guo Q; Manolopoulou M; Bian Y; Schilling AB; Tang WJ, Molecular basis for the recognition and cleavages of IGF-II, TGF-alpha, and amylin by human insulin-degrading enzyme. J. Mol. Biol 2010, 395 (2), 430–43. [PubMed: 19896952]

14. Mukherjee A; Song E; Kihiko-Ehmann M; Goodman JP Jr.; Pyrek JS; Estus S; Hersh LB, Insulysin hydrolyzes amyloid beta peptides to products that are neither neurotoxic nor deposit on amyloid plaques. J. Neurosci 2000, 20 (23), 8745–9. [PubMed: 11102481]

15. Libich DS; Fawzi NL; Ying J; Clore GM, Probing the transient dark state of substrate binding to GroEL by relaxation-based solution NMR. Proc. Natl. Acad. Sci. U.S.A 2013, 110 (28), 11361–11366. [PubMed: 23798407]

16. Tugarinov V; Clore GM, Exchange saturation transfer and associated NMR techniques for studies of protein interactions involving high-molecular-weight systems. J. Biomol. NMR 2019, 73 (8–9), 461–469. [PubMed: 31407202]

17. Skrynnikov NR; Dahlquist FW; Kay LE, Reconstructing NMR spectra of "invisible" excited protein states using HSQC and HMQC experiments. J. Am. Chem. Soc 2002, 124 (41), 12352–12360. [PubMed: 12371879]

18. Palmer AG, Chemical exchange in biomacromolecules: Past, present, and future. J. Magn. Reson 2014, 241, 3–17. [PubMed: 24656076]

19. McConnell HM, Reaction rates by nuclear magnetic resonance. J. Chem. Phys 1958, 28 (3), 430–431.

20. McCord LA; Liang WG; Dowdell E; Kalas V; Hoey RJ; Koide A; Koide S; Tang W-J, Conformational states and recognition of amyloidogenic peptides of human insulin-degrading enzyme. Proc. Natl. Acad. Sci. U.S.A 2013, 110 (34), 13827–13832. [PubMed: 23922390]

21. Wälti MA; Steiner J; Meng F; Chung HS; Louis JM; Ghirlando R; Tugarinov V; Nath A; Clore GM, Probing the mechanism of inhibition of amyloid-β(1–42)–induced neurotoxicity by the chaperonin GroEL. Proc. Natl. Acad. Sci. U.S.A 2018, 115 (51), E11924–E11932. [PubMed: 30509980]

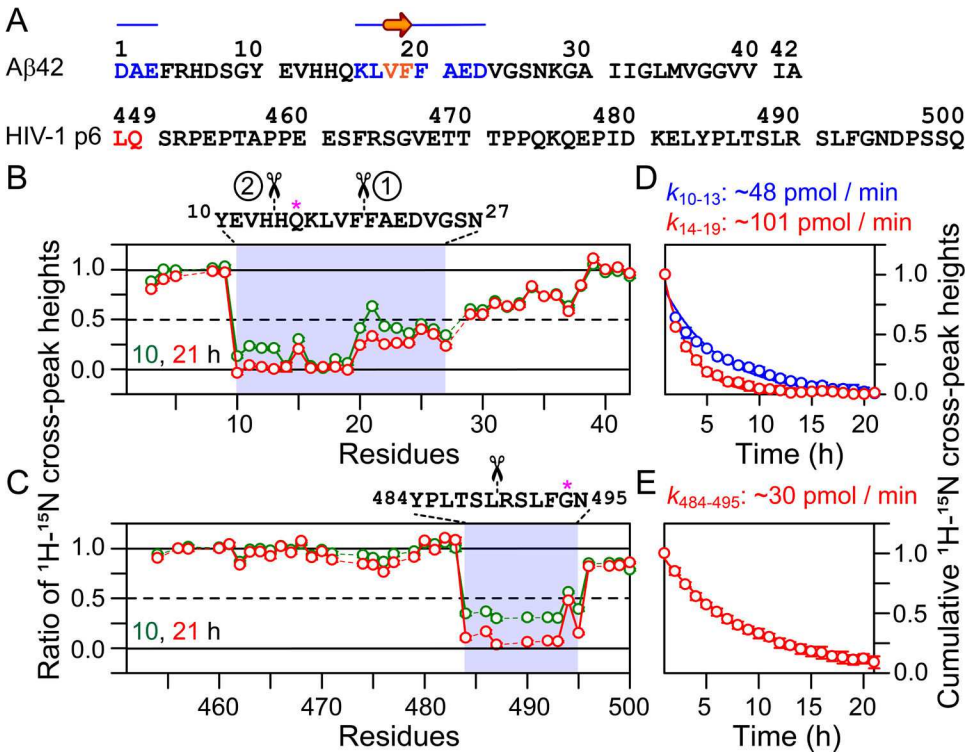

Figure 1. Digestion of Aβ42 and p6 by IDE at 2 °C.

(A) Primary sequences of Aβ42 and p6 (Aβ40 lacks the last two C-terminal residues). IDE-bound Aβ42 residues that are visible in the corresponding crystal structure[13] are marked in blue; residues in orange form a β-strand in the active site of IDE. p6 used in current study lacks the two N-terminal residues (red). Time course of the reduction in $^{1}H_{N}/^{15}N$ cross-peak heights of 50 μM ^{15}N-labeled (B) Aβ42 and (C) p6 on addition of 10 μM IDE (all reported IDE concentrations are in monomeric subunits). Affected regions are highlighted (blue rectangles). Cleavage sites are marked. For Aβ42, the circled numbers indicate the cleavage order. Decay of cumulative cross-peak heights of (D) Aβ42 and (E) p6 upon hydrolysis. Residues 10–13 (blue) and 14–19 (red; without outlier Q15) of Aβ42 and 484–495 of p6 (without G494) were used for calculating averages. The curves were fit to the equation $y = ae^{-kt}$.

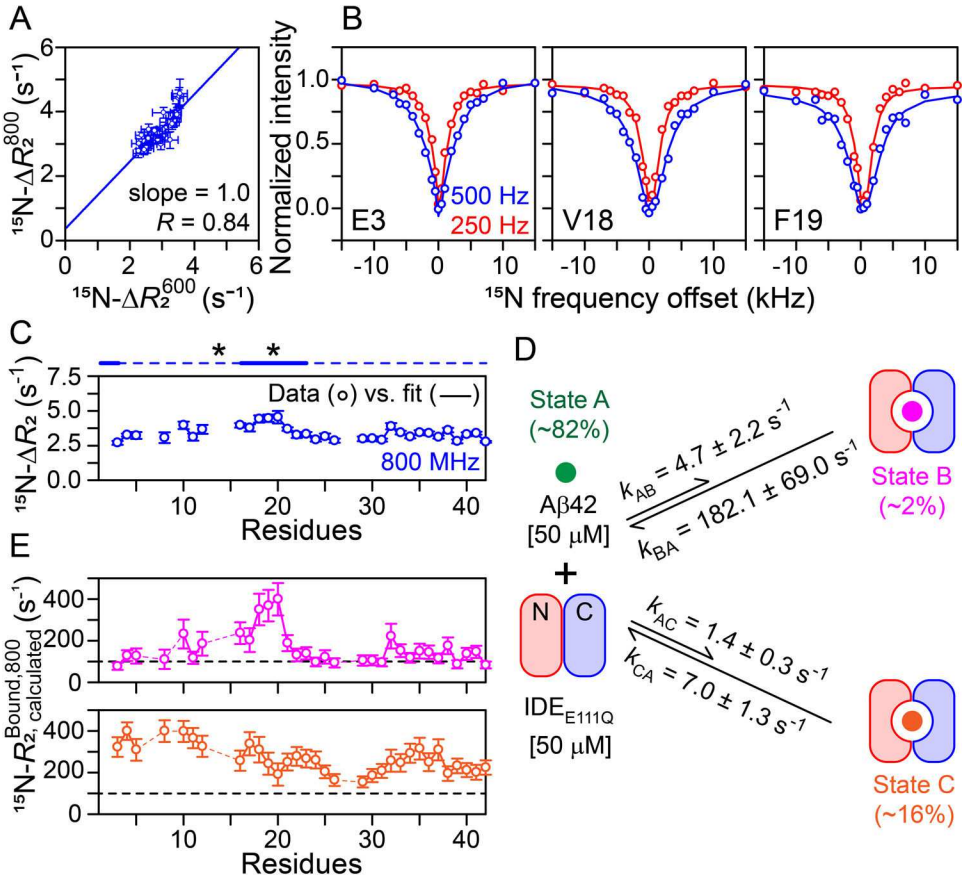

Figure 2. NMR analyses of Aβ42 – IDE_{E111Q} interactions at 2 °C.

(A) Field-dependence between ^{15}N-ΔR_2 values of ^{15}N-labeled Aβ42 with IDE_{E111Q} (50 μM each) recorded at 600 and 800 MHz. (B) Representative ^{15}N-DEST profiles at two CW-RF fields and (C) ^{15}N-ΔR_2 profiles measured on Aβ42 + IDE_{E111Q} sample (50 μM each) at 800 MHz; experimental data in circles, and best fits by the solid lines. IDE-bound residues visible in the crystal structure[13] are shown by solid blue lines above (C). The locations of cleavage sites are marked by asterisks (cf. Figure 1B). (D) Summary of kinetic and population parameters obtained from best fitting of all NMR data to a three-state exchanging system. A monomeric subunit of IDE_{E111Q} dimer is shown. (E) ^{15}N-R_2^{Bound} profiles for IDE-bound Aβ42 for State **B** (pink) and State **C** (orange) at 800 MHz obtained from the fits.

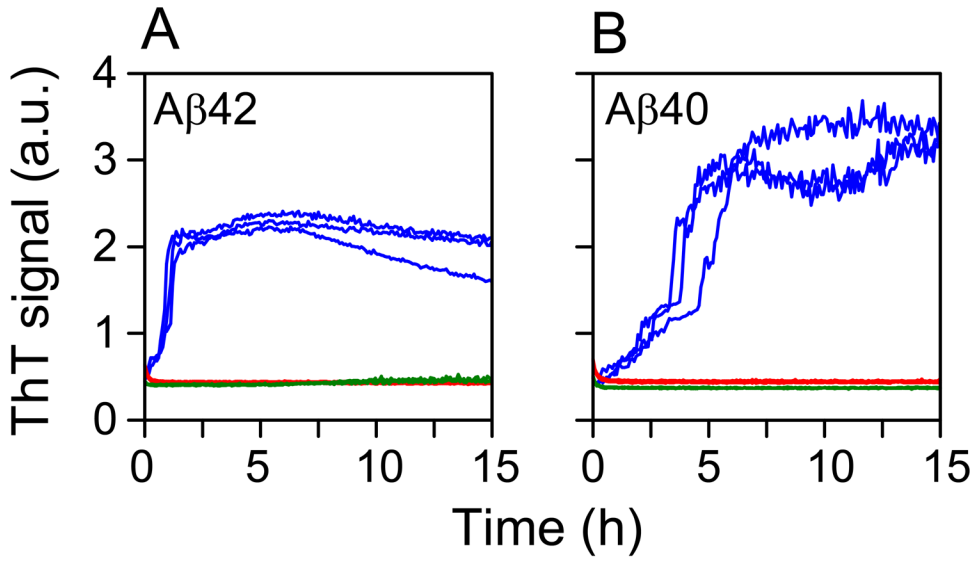

Figure 3. Aggregation of Aβ at 37 °C studied by Thioflavin T (ThT) assays.

10 μM (A) Aβ42 and (B) Aβ40 were incubated without (blue) and with 1 μM IDE (red) and IDE_{E111Q} (green); $n = 3$.

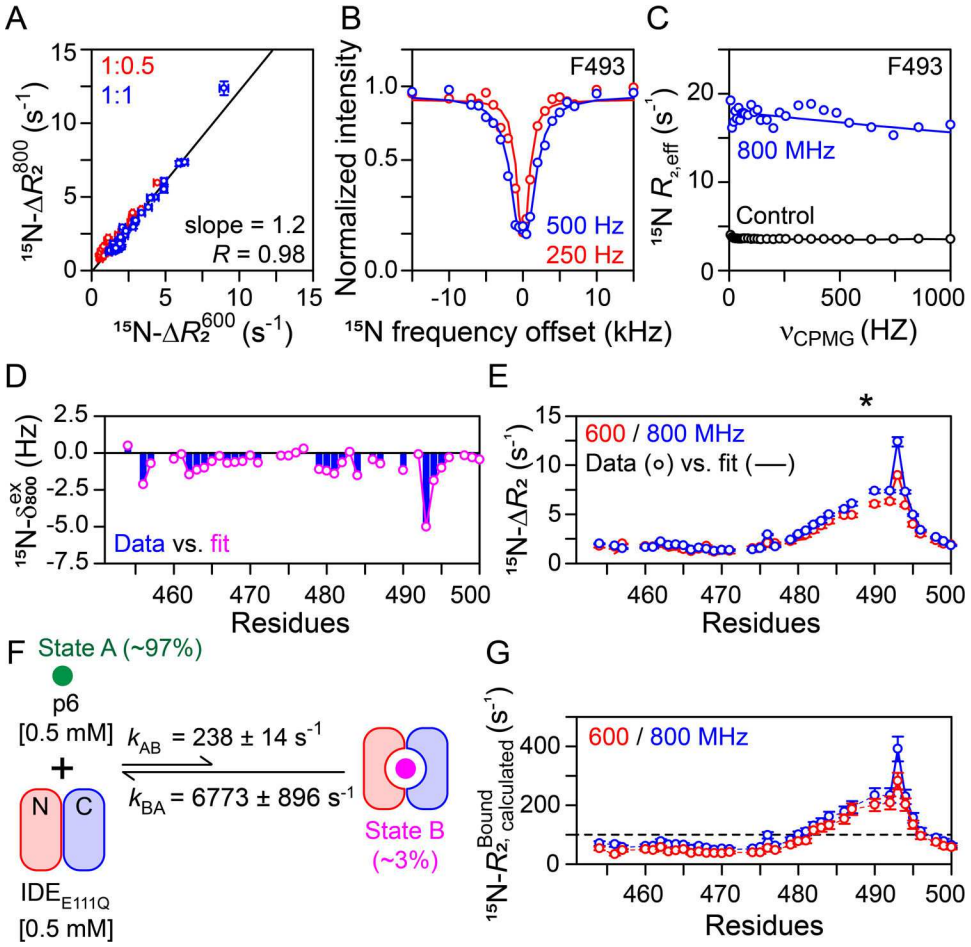

Figure 4. NMR analyses of p6 – IDE$_{E111Q}$ interactions at 2 °C.

(A) Field-dependence between ^{15}N-ΔR_2 values of 0.5 mM ^{15}N-labeled p6 in the presence of 0.25 (red) and 0.5 mM (blue) IDE$_{E111Q}$; 600 and 800 MHz. Representative (B) ^{15}N-DEST profiles and (C) ^{15}N-CPMG dispersions recorded on p6 + IDE$_{E111Q}$ sample (0.5 mM each; 800 MHz; experimental data in circles, and best fits by the solid lines). (D) Observed (bars) against calculated (circles) ^{15}N-δ^{ex} values (800 MHz) and (E) ^{15}N-ΔR_2 profiles measured on p6 + IDE$_{E111Q}$ sample (0.5 mM each) at 800 (blue) and 600 (red) MHz. Asterisk denotes the cleavage site (cf. Figure 1C). (F) Summary of kinetic and population parameters obtained from best fitting all NMR data to a two-state exchange model. (G) ^{15}N-R_2^{Bound} profiles of IDE-bound p6 at 600 (red) and 800 (blue) MHz obtained from the fits.